JACS
JOURNAL OF THE AMERICAN CHEMICAL SOCIETY

ARTICLE

pubs.acs.org/JACS

Inorganic Supramolecular Compounds with 3-D Chiral Frameworks Show Potential as Both Mid-IR Second-Order Nonlinear Optical and Piezoelectric Materials

Xiao-Ming Jiang,[†,‡] Ming-Jian Zhang,[†] Hui-Yi Zeng,[†] Guo-Cong Guo,[*,†] and Jin-Shun Huang[†]

[†]State Key Laboratory of Structural Chemistry, Fujian Institute of Research on the Structure of Matter, Chinese Academy of Sciences, Fuzhou 350002, P. R. China

[‡]Graduate School of Chinese Academy of Sciences, Beijing 100039, P. R. China

Supporting Information

ABSTRACT: Two inorganic supramolecular compounds, $(Hg_6P_3)(In_2Cl_9)$ (**1**) and $(Hg_8As_4)(Bi_3Cl_{13})$ (**2**), which have chiral 3-D host frameworks with guest moieties filling the helical tunnels, have been synthesized. They both have large second-harmonic generation efficiencies, and compound **2** also exhibits obvious single-crystal piezoelectric performance. Theoretical studies from first-principles calculations were performed on their nonlinear optical (NLO) and piezoelectric properties, and results indicate that good NLO and piezoelectric materials can be obtained by designing both complicated polycations and polyanions with large molecular polarizability as functional components rather than traditional single polyanions.

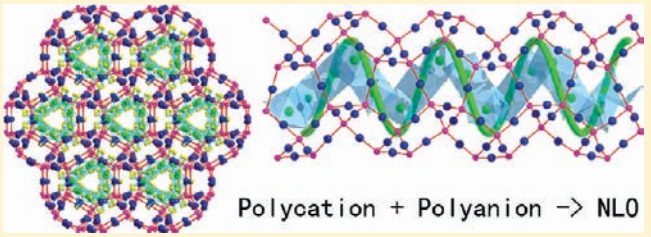

1. INTRODUCTION

Second-order nonlinear optical (NLO) materials are of current interest and great importance owing to their uses in optical signal processing and new laser sources based on the NLO processes of second-harmonic generation (SHG) and optical parametric oscillation.[1] Although considerable progress has been made recently in the exploration of new NLO materials,[2] many of them, based on well-known oxides such as KH_2PO_4 (KDP), $KTiOPO_4$ (KTP), β-BaB_2O_4 (BBO), LiB_3O_5 (LBO), and so on,[3] which are widely used in the visible and ultraviolet region, cannot be used in the mid- and far-IR regions because of strong absorption. Until now, NLO material systems used worldwide for IR have mainly included ABC_2 chalcopyrite and wurtzite-type compounds like $ZnGeP_2$,[4a] $AgGaS_2$,[4b] and $LiInS_2$,[4c] AMX_3-type metal halides like $CsGeCl_3$[5a] and $CsCdBr_3$,[5b] iodate compounds like $M^{II}(IO_3)_2$ (M = Mg, Mn, Co, Zn, Hg)[6a] and NaI_3O_8,[6b] and other chalcogenidometalates like $Li_2Ga_2GeS_6$,[7a] α- and β-$A_2Hg_3M_2S_8$ (A = K, Rb; M = Ge, Sn),[2c] $A_2P_2Se_6$ (A = K, Rb),[7b] $HgGa_2S_4$,[7c] $BaGa_4S_7$,[2i] $A_3Ta_2AsS_{11}$ (A = K, Rb),[7d] $ZnY_6Si_2S_{14}$,[2k] and $La_6MgGe_2S_{14}$.[7e] However, commercially available IR NLO materials like $ZnGeP_2$ and $AgGaS_2$ are not good enough for high-power applications, mainly due to their low laser damage thresholds, and most of the other IR NLO material systems are just at the stage of laboratory research. Therefore, the search for new material systems with excellent IR NLO performance has become a key area of research in NLO material science and laser technology.[8]

Supramolecular compounds are aggregates of well-defined composition and structure consisting of two or more different building blocks, in which species of different structures and functions can be assembled into mixed framework compounds that are likely to exhibit diverse structures, improved properties, and unique functions that cannot be obtained from the pure building blocks alone.[9] Although supramolecular chemistry has been of great interest in the past two decades,[10] and lots of supramolecular compounds have been synthesized, relatively few of them are found to have a chiral 3-D host framework with helical tunnels that can capture guest moieties, except for some organic supramolecular compounds, aluminosilicate zeolites, and polyoxometalates. Herein, we report two inorganic supramolecular compounds, $(Hg_6P_3)(In_2Cl_9)$ (**1**) and $(Hg_8As_4)(Bi_3Cl_{13})$ (**2**), with chiral 3-D frameworks, and show large SHG efficiencies for **1** and **2** and single-crystal piezoelectric performance for **2**.

2. EXPERIMENTAL SECTION

Reagents and Syntheses of 1 and 2. Red phosphorus was washed with a 30% aqueous solution of KOH, water, and ethanol (twice) and then vacuum-dried; all the other starting materials were used as received without further purification. Single crystals of the two compounds were obtained by solid-state reactions. Compound **1** was crystallized from a reaction mixture containing $HgCl_2$ (0.6 mmol, 99.5%), Hg_2Cl_2 (0.3 mmol, 99.5%), In (0.4 mmol, 99.99%), and red phosphorus P (0.6 mmol, 98.5%). Compound **2** was crystallized from a reaction mixture containing Hg_2Cl_2 (0.8 mmol, 99.5%), $BiCl_3$ (0.6 mmol, 98%), and As (0.8 mmol, 99.999%). The starting materials were ground into fine powders in an agate mortar and pressed into pellets.

Received: September 2, 2010
Published: February 22, 2011

They were then loaded into Pyrex tubes which were evacuated to 1×10^{-4} Torr and flame-sealed. The tubes were placed into a computer-controlled furnace, heated from room temperature to 200 °C at a rate of 50 °C/h, and kept at 200 °C for 2 days. The tubes were next heated to 430 at 20 °C/h, kept at 430 °C for 5 days, and then slowly cooled to 100 °C at a rate of 2.5 °C/h. They were finally cooled to room temperature in 5 h. All the samples (yellow block crystals) of **1** and **2** used for various measurements were first hand-picked under a microscope and then washed several times with water and alcohol by ultrasonic cleaning, and their purities were confirmed in an X-ray diffraction (XRD) study. Compounds **1** and **2** are stable in red light but sensitive to ambient or fluorescent light when exposed to near-UV light for a long time, and the surfaces of crystals of **2** turn black quickly upon irradiation by UV light.

Caution! *$HgCl_2$, Hg_2Cl_2, and As are very toxic. Extreme care must be exercised, and some toxic gases may be released after the Pyrex tubes are opened. $HgCl_2$ and $BiCl_3$ are water-sensitive, so weighing reagents, grinding the mixture, and pressing into pellets should be performed in a drybox.*

A single crystal of **2** suitable for piezoelectric measurement was prepared by chemical vapor deposition. The starting materials, Hg_2Cl_2 (1.2 mmol, 99.5%), $BiCl_3$ (0.9 mmol, 98%), and As (1.2 mmol, 99.999%), were ground into a fine powder in an agate mortar and pressed into a pellet. The pellet was then loaded into one end of a very clean quartz tube, about 15 cm long and 11 mm in diameter, which was evacuated to 1×10^{-4} Torr, and flame-sealed. The quartz tube was placed into a computer-controlled furnace to allow an obvious temperature gradient. The hot end, containing reactants, was kept at 380 °C for 48 h and then slowly cooled to 180 °C at a rate of 2.0 °C/h, while the cold end was kept at 370 °C and then synchronously cooled to 170 °C. Several big single crystals of **2** were found at the cool end of the quartz tube.

Crystal Structure Determinations of 1 and 2. For **1** and **2**, single crystals with dimensions of $0.05 \times 0.02 \times 0.02$ mm^3 and $0.10 \times 0.04 \times 0.04$ mm^3, respectively, were mounted on a glass fiber for single-crystal XRD analysis. The measurements were performed on a Rigaku Saturn 70/mercury CCD diffractometer equipped with graphite-monochromated Mo Kα radiation (λ = 0.71073 Å) at 293 K. The intensity data sets were collected with an ω-scan technique and reduced using CrystalClear software.[11]

The structures of **1** and **2** were solved by direct methods and refined by full-matrix least-squares techniques on F^2 with anisotropic thermal parameters for all atoms. All of the calculations were performed with the Siemens SHELXL version 5 package of crystallographic software.[12] The formulas take collectively into account crystallographically refined compositions and requirements of charge neutrality. Relevant crystallographic data and details of the experimental condition for $(Hg_6P_3)(In_2Cl_9)$ and $(Hg_8As_4)(Bi_3Cl_{13})$ are summarized in Table 1. Atomic coordinates and selected interatomic distances are reported in Tables S1−S4 in the Supporting Information.

Powder XRD. The powder XRD patterns (Supporting Information, Figure S1) were collected with a Rigaku DMAX 2500 diffractometer at 40 kV and 100 mA for Cu Kα radiation (λ =1.5406 Å) with a scan speed of 2°/min at room temperature. The simulated patterns were produced using the Mercury program and single-crystal reflection data.

Energy-Dispersive X-ray Spectroscopy (EDS). Semi-quantitative microscope analysis using EDS were performed on a JSM6700F scanning electron microscope on a single crystal, which confirmed the presence of Hg, In, P, and Cl in the approximate molar ratio 6.0:2.1:3.3:9.0, and Hg, Bi, As, and Cl in the approximate molar ratio 8.0:3.3:3.3:12.0, for **1** and **2**, respectively. No other elements were detected.

Thermogravimetric Analysis (TGA) and Mass Spectrum Analysis (MSA). Thermogravimetric/direct temperature analysis mass spectrometry (TG/DTA-MS) studies of **1** and **2** were carried out with a Thermal Analysis STA 400C-QMS 403C quadrupole mass spectrometer under a nitrogen atmosphere. The sample and reference were held in Al_2O_3 crucibles and heated at a rate of 10 °C/min from room temperature to 1000 °C with a Netzsch STA 449C instrument, and the thermal decomposition products of **1** and **2** were transported into a QMS 403C instrument. Some possible molecular fragments of thermal decomposition products of **1** (formula weights 35.5, 71, 102, 115, 146) and **2** (formula weights 35.5, 71, 75, 201, 209, 272) were checked.

Table 1. Crystal Data and Structure Refinement Parameters for $(Hg_6P_3)(In_2Cl_9)$ and $(Hg_8As_4)(Bi_3Cl_{13})$

chemical formula	$(Hg_6P_3)(In_2Cl_9)$ (**1**)	$(Hg_8As_4)(Bi_3Cl_{13})$ (**2**)
formula weight	1845.14	2992.19
crystal size (mm^3)	0.05 × 0.05 × 0.05	0.10 × 0.04 × 0.04
crystal system	monoclinic	trigonal
space group	$P2_1$	$P3_121$
a (Å)	10.3014(11)	11.3324(4)
b (Å)	10.6935(8)	11.3324(4)
c (Å)	10.8370(12)	42.768(4)
β (°)	116.249(4)	
V (Å^3)	1070.68(18)	4756.6(5)
Z	2	6
D_{calcd} (g cm^{-1})	5.723	6.267
μ (mm^{-1})	46.287	60.383
F(000)	1552	7452
θ range (°)	2.10−27.42	2.13−25.50
index range	$-13 \le h \le 13$	$-12 \le h \le 13$
	$-13 \le k \le 13$	$-13 \le k \le 13$
	$-13 \le l \le 14$	$-44 \le l \le 51$
measd reflns	9374	30458
indep reflns/R_{int}	4414/0.0939	5920/0.1227
obsd reflns	4116	5490
$R1^a$ ($I > 2\sigma(I)$)	0.0592	0.0499
w$R2^b$ (all data)	0.1185	0.1179
GOF on F^2	1.011	1.029
Flack parameter	0.00(1)	−0.008(14)
$\Delta\rho_{max}/\Delta\rho_{min}$ (e/Å^3)	3.601/−3.394	2.257/−4.416

$^a R1 = ||F_o| - |F_c||/|F_o|$. $^b wR^2 = [w(F_o^2 - F_c^2)^2]/[w(F_o^2)^2]^{1/2}$.

Infrared and UV−Vis−NIR Diffuse Reflectance Spectroscopies. The diffuse reflectance spectra were recorded at room temperature on a computer-controlled Lambda 900 UV−vis−NIR spectrometer equipped with an integrating sphere in the wavelength range of 300−1700 nm. A $BaSO_4$ plate was used as a reference, on which the finely ground powders of the samples were coated. The absorption spectra were calculated from reflection spectra using the Kubelka−Munk function.[13] The IR spectra were recorded by using a Nicolet Magana 750 FT-IR spectrophotometer in the range of 4000−400 cm^{-1}. Powdery samples were pressed into pellets with KBr. No FT-IR absorption peaks of **1** and **2** appear in the range 4000−400 cm^{-1}.

SHG Measurements of 1 and 2 and Piezoelectricity Measurement of 2. Powder SHG measurements on hand-selected crystalline samples were performed on a modified Kurtz-NLO system using 2.1 μm laser radiation. The output signals were detected by a photomultiplier, and $AgGaS_2$ powder sieved with 150 meshes (~100 μm) was used for comparison. Compounds **1** and **2** were ground and sieved into several distinct particle size ranges (0−50, 50−76, 76−100, 100−150, 150−200, and 200−300 μm). All of the samples were pressed between glass microscope cover slides and secured with tape in 1-mm-thick

aluminum holders containing an 8-mm-diameter hole. A single crystal of **2** was orientated using an X-ray diffractometer and then cut into dimensions of 1.0 × 2.0 × 5.0 mm^3 along the ⟨001⟩ direction. The piezoelectric coefficient was measured using a piezo-d_{33} meter.

Computational Descriptions. Theoretical calculations including band structure, second-order NLO susceptibility, and piezoelectric constants were based on the methods of density functional theory[14] (DFT) and density functional perturbation theory[15] (DFPT), which have proven to be rather successful for describing the dielectric, piezoelectric, and NLO properties of a wide range of materials in which electronic correlation is not too strong.[16] The calculations were performed using the ABINIT computer code package.[17]

DFPT calculations were carried out using the Fritz-Haber Institute pseudopotentials scheme (Troullier−Martins scheme)[18] with a plane-wave energy cutoff of 20 and 12 hartree for **1** and **2**, respectively. Monkhorst−Pack grids for Brillouin-zone *k*-point sampling used in the calculations were 3×2×3 for **1** and 3×3×2 for **2**. The exchange and correlation effects were treated by the local-density approximation (LDA) in the Ceperley−Alder form with the Perdew−Wang parametrization.[19] Convergence of the calculated properties was verified with respect to the *k*-point sampling and plane-wave energy cutoff.

In the calculation of optical properties and density of states (DOS) of **1** and **2**, scissors operators of 0.83 and 0.60 eV were applied for **1** and **2**, respectively, and more than 300 and 600 empty bands were used for **1** and **2**, respectively.

In the calculation of full piezoelectric tensors, we use the perturbation theory within the DFT of the second derivatives of the total energy of periodic solids with respect to (i) the collective displacements of atoms with different wave vectors and (ii) homogeneous static electric fields. The calculated full piezoelectric tensors can be decomposed into "clamped-ion" and "internal-strain" contributions, expressed as follows:[20]

$$\begin{aligned} e_{ij} &= e_{ij,\mathrm{c}} + \frac{ea}{\Omega}\sum_{km} Z_{im}(k)\,\frac{\mathrm{d}u_m(k)}{\mathrm{d}\eta_j} \\ &= e_{ij,\mathrm{c}} + \frac{ea}{\Omega}\sum_{km} Z_{im}(\text{host atoms})\,\frac{\mathrm{d}u_m(\text{host atoms})}{\mathrm{d}\eta_j} \\ &\quad + \frac{ea}{\Omega}\sum_{km} Z_{im}(\text{guest atoms})\,\frac{\mathrm{d}u_m(\text{guest atoms})}{\mathrm{d}\eta_j} \\ &= e_{ij,\mathrm{c}} + e_{ij,\mathrm{int,host}} + e_{ij,\mathrm{int,guest}} = e_{ij,\mathrm{c}} + e_{ij,\mathrm{int}} \end{aligned}$$

where *k* runs over all the atoms in the unit cell, *m* (*m* = 1, 2, 3) runs over all the three displacement directions, *a* and Ω are the equilibrium lattice constant along the *a*-direction and the volume of the primitive cell, respectively, and *e* is the magnitude of the electron charge. The clamped-ion coefficient $e_{ij,c}$ measures the contributions to e_{ij} of vanishing internal strain, which is associated with internal atomic coordinates frozen at their equilibrium positions. $Z_{im}(k)$ is the Born effective charge of the atom *k* in the *i*-direction, and $\mathrm{d}u_m(k)/\mathrm{d}\eta_j$ characterizes the response of the *k*th atom's internal coordinate along the *m*-direction to the macroscopic strain η_j. The piezoelectric coefficient with respect to internal strain, denoted $e_{ij,\mathrm{int}}$, is equal to $(ea/\Omega)\sum_{km} Z_{im}(k)\,\mathrm{d}u_m(k)/\mathrm{d}\eta_j$ and can be divided into the contributions of the host and guest parts, $e_{ij,\mathrm{int,host}}$ and $e_{ij,\mathrm{int,guest}}$, respectively.

3. RESULTS AND DISCUSSION

The crystal structure of **1** features a 3-D cationic host framework and discrete guest anions (Figure 1a). The 3-D cationic network is built up from approximately linearly coordinated mercury and tetrahedrally coordinated phosphorus atoms to form a helical HgP spring (Figure 2a). Two concentric HgP springs are bridged by Hg2, Hg4, and Hg6 atoms through Hg−P bonds to form a cylinder with a 1-D helical tunnel along the *b*-direction, and then the helical cylinders share all the mercury and phosphorus atoms with each other to form a 3-D honeycomb-like $(Hg_6P_3)^{3+}$ framework (Figure 1a). As determined by TOPOS,[21] the Schäfli symbol of this 4-connected uninodal network is $5^5 8$.

The host structure of **2** is similar to that of **1**, built up instead from mercury and arsenic atoms to form a $(Hg_8As_4)^{4+}$ framework (Figure 1b), which is more distorted than that of **1**. Linearly coordinated mercury and tetrahedrally coordinated arsenic atoms form a distorted helical HgAs spring (Figure 2b). Two concentric HgAs springs are bridged by four (rather than three as in **1**) crystallographically independent Hg2, Hg4, Hg6, and Hg7 atoms through Hg−As bonds to form a cylinder with a 1-D helical tunnel along the *c*-direction, and then the helical cylinders share all the mercury and arsenic atoms with each other to form a 3-D honeycomb-like $(Hg_8As_4)^{4+}$ framework (Figure 2b), whose Schäfli symbol is also $5^5 8$.

The guest anion of **1** is built up from distorted $(InCl_6)^{3-}$ octahedra, two of which face-share with each other to form a fused $(In_2Cl_9)^{3-}$ anion. Correspondingly, the guest polyanion of **2** is built up from octahedrally and pentagonal bipyramidally coordinated bismuth to form a distorted $(BiCl_6)^{3-}$ octahedron and $(BiCl_7)^{4-}$ pentagonal bipyramid, respectively, which edge-share with each other in 2:1 ratio to form a quasi-1-D infinite $^1_\infty(Bi_3Cl_{13})^{4-}$ helical chain. The discrete $(In_2Cl_9)^{3-}$ anions and the $^1_\infty(Bi_3Cl_{13})^{4-}$ helical chains are embedded in the channels of the host frameworks of **1** and **2**, respectively (Figure 1, right).

On the other hand, the crystal structure of **2** can be well related to that of **1**. Because all Hg and As atoms in **2** have nearly the same coordination geometry as the Hg and P atoms in **1**, respectively, the minimum repeating unit of the highly topologically symmetric host part in **2** can be truncated as $(Hg_6As_3)^{3+}$, like the minimum repeating unit $(Hg_6P_3)^{3+}$ in **1**. The minimum repeating unit of the guest part in **2**, $(Bi_3Cl_{13})^{4-}$, is tripled because of a 3_1 helical axis along the $^1_\infty(Bi_3Cl_{13})^{4-}$ polyanions, and the minimum repeating unit of the host part in **2**, $(Hg_6As_3)^{3+}$, is quadrupled to achieve charge balance, forming an integral unit cell whose volume is about 4 times that of **1**. In contrast, **1** requires only one unit each of $(Hg_6P_3)^{3+}$ and $(In_2Cl_9)^{3-}$ to achieve charge balance.

The Hg−P bond lengths in the cationic moiety in **1** range from 2.373(7) to 2.406(7) Å (Supporting Information, Figure S6), within the normal range for Hg−P bond lengths in known mercury pnictide halides.[22] The In−Cl bond distances (2.397(7)−2.699(7) Å) are close to those found in indium halides.[23] Correspondingly, the Hg−As bond lengths in **2** range from 2.461(2) to 2.497(2) Å, within the normal range for Hg−As bond lengths,[24] and the Bi−Cl bond distances (2.503(3)−2.823(3) Å) are close to those found in bismuth halides.[25]

Unlike $Hg_4As_2Br_3$, $Hg_{7.4}As_4Cl_6$, Hg_2PCl_2, Hg_2P_3Br, $Hg_7P_4Br_6$, $Hg_9I_6P_5$, and so on,[26] in which some or all P or As atoms join into pairs to form Z_2^{4-} (Z = P, As) dumbbells coordinated by six Hg^{2+} cations, there are no P−P or As−As bonds in **1** and **2**, and only Z^{3-} (Z = P, As) anions coordinated by four Hg^{2+} cations are present in the host frameworks of **1** and **2**.

The distances between the cationic hosts and anionic guests in the present compounds are significantly longer than the expected values for covalent bonding, thus suggesting the typical supramolecular interactions between them.[9] The shortest interatomic distances between the chlorine atoms of the guest anions and the mercury atoms in the host frameworks of **1** and **2** are 3.04 and

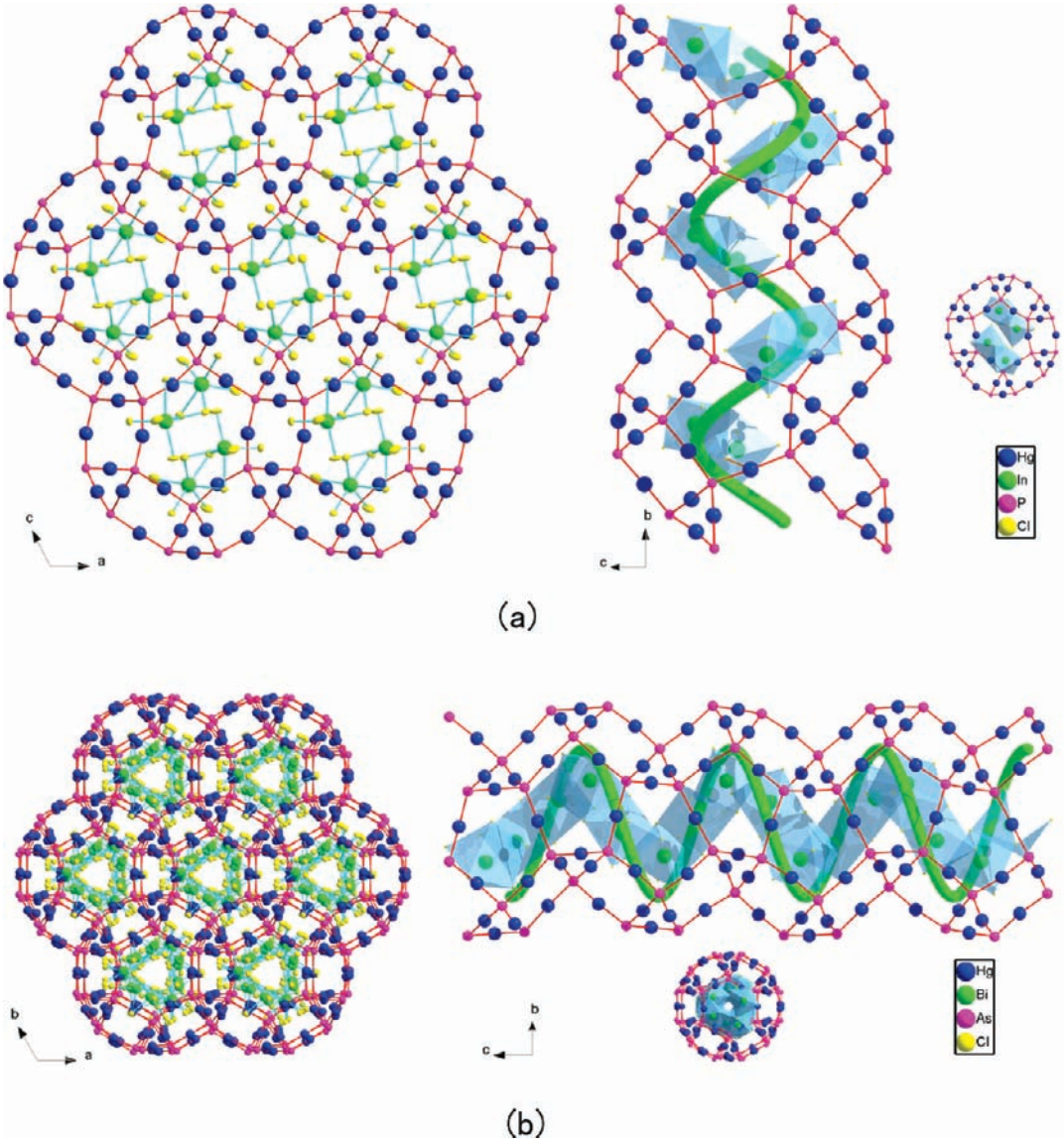

Figure 1. (a) View of 3-D cationic host $(Hg_6P_3)^{3+}$ framework and discrete guest $(In_2Cl_9)^{3-}$ anions of **1** along the *b*-direction (left); isolated $(In_2Cl_9)^{3-}$ anions are embedded in the helical channels of the host framework (right). (b) View of 3-D cationic host $(Hg_8As_4)^{4+}$ framework and $^1_\infty(Bi_3Cl_{13})^{4-}$ helical chain of **2** along the *c*-direction (left); $^1_\infty(Bi_3Cl_{13})^{4-}$ helical chain is embedded in the channel of the host framework (right).

2.94 Å, respectively, which are much longer than the Hg−Cl covalent bond length but shorter than the sum of the van der Waals radii of Hg and Cl atoms. This indicates that there are weak supramolecular interactions between the cationic and anionic moieties in the crystal structures of **1** and **2**, as found in the literature.[23,25]

The SHG signals as a function of particle size from the measurements made on ground crystals of **1** and **2** are shown in Figure 3. The results are consistent with type-I phase-matching behavior according to the rule proposed by Kurtz and Perry.[27] It is well known that the SHG signal intensity measured by the Kurtz and Perry powder method is proportional to the square of the second-order nonlinear d_{eff} coefficient, and the second-order susceptibility $\chi^{(2)}_{eff}$ is twice the SHG coefficient d_{eff}. The measured SHG signal intensities of **1** and **2** are about 0.5 and 1.2 times that of $AgGaS_2$, respectively, and the reported d_{eff} coefficient for AGS is 12.5 pm/V (3.0×10^{-8} esu),[28] so the derived second-order susceptibilities $\chi^{(2)}_{eff}$ for **1** and **2** are 17.68 pm/V (4.24×10^{-8} esu) and 27.38 pm/V (6.57×10^{-8} esu), respectively, which are approximately 20 and 31 times as large as $\chi^{(2)}_{36}$ (KDP, 0.88 pm/V), respectively.

The piezoelectric coefficient of **2** with single-crystal dimensions of $1.0 \times 2.0 \times 5.0$ mm^3 along the ⟨001⟩ direction was measured using a piezo-d_{33} meter to yield $d_{11} = 3.2$ pC/N, which is larger than that of the most well-known piezoelectric material quartz ($d_{11} = -2.31$ pC/N).[29]

The IR and optical diffuse reflectance spectra show that compounds **1** and **2** are transparent in the IR range (0.6−25 μm) (Supporting Information, Figures S2 and S3), similar to the well-known IR NLO crystals $AgGaS_2$ (0.48−11.4 μm) and $ZnGeP_2$ (0.74−12 μm). Therefore, compounds **1** and **2** may be good candidates for mid- and far-IR NLO materials. Generally, laser damage thresholds of NLO materials are proportional to their band gaps, increasing with an increase in band gap. The optical diffuse reflectance spectra indicate optical band gaps of 3.13 eV for **1** and 2.43 eV for **2** (Supporting Information, Figure S4),

dx.doi.org/10.1021/ja107921a |*J. Am. Chem. Soc.* 2011, 133, 3410–3418

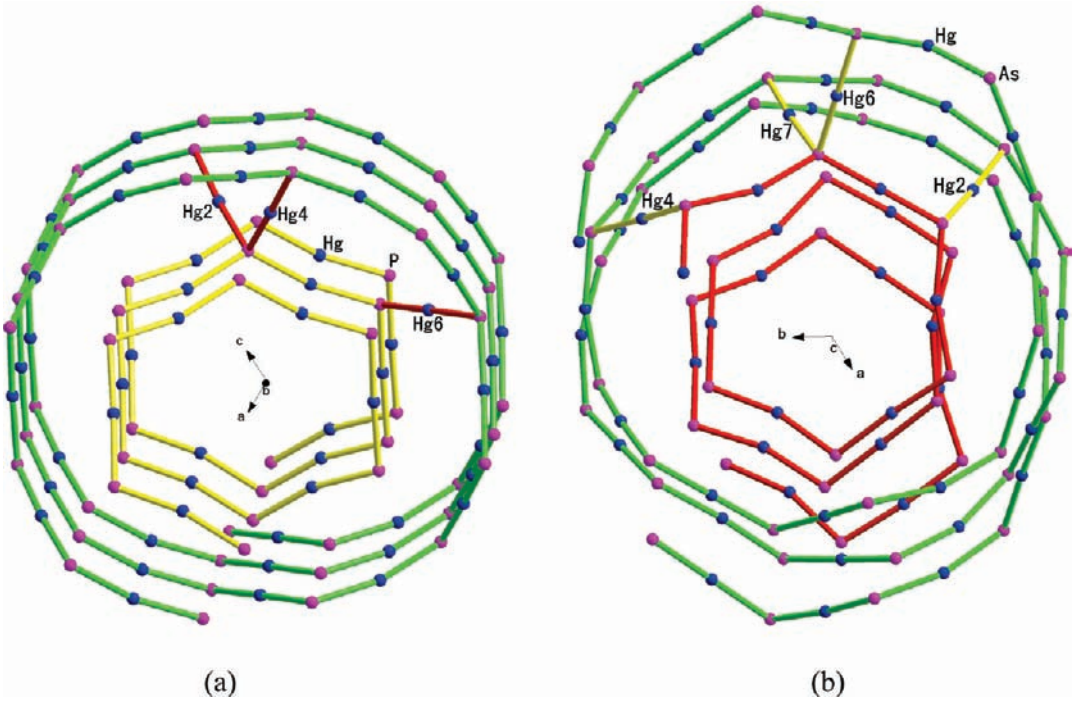

Figure 2. Topology of the host parts of **1** (a) and **2** (b). Concentric HgP(As) springs and bridging Hg−P(As) bonds are distinguished by three different colors.

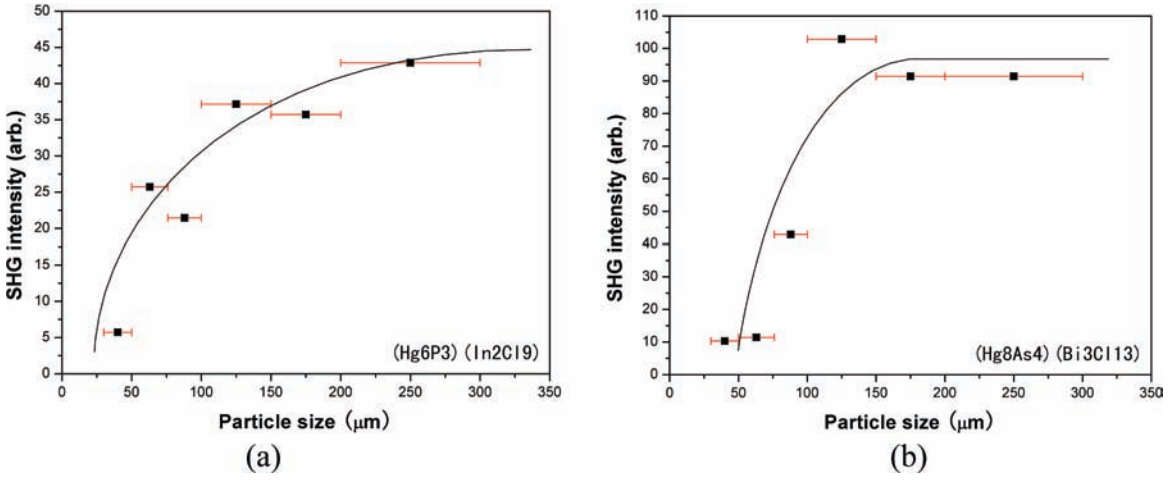

Figure 3. Phase-matching results for **1** (a) and **2** (b). The curve is to guide the eye and is not a fit to the data.

which are comparable with those of $AgGaS_2$ (2.73 eV) and $ZnGeP_2$ (2.0 eV),[4] implying that the present compounds have laser damage thresholds comparable to those of known materials.

The TGA curves show that compounds **1** and **2** are stable up to 280 and 200 °C, respectively (Supporting Information, Figure S5), and then both continually lose weight up to about 430 °C. The total weight loss at 1000 °C is 94.1% and 84.4% for **1** and **2**, respectively. Some possible thermal decomposition products are checked by MSA, and the final residues are characterized by EDS analysis. Cl^-, Hg^+, and PCl_2^+ ions are detected by MSA during the heating of **1**, and its final residue contains only the elements phosphorus and indium in a ratio of about 2:1. For **2**, only Hg^+, and no Cl^- ion, is detected during the heating, and the final residue contains only the element bismuth.

The larger SHG efficiency of **2** than **1** results from the larger average bond orders[30] of Hg−As bonds (1.36) than Hg−P bonds (1.19), of and Bi−Cl bonds (0.63) than In−Cl bonds (0.49), which are of the hosts and guests of **2** and **1**, respectively.[31] Therefore, an IR NLO material of larger SHG efficiency can be obtained by introducing some atoms with higher polarization in hosts and guests, which can be easily realized via supramolecular synthesis. Generally speaking, supramolecular synthesis is easier than conventional molecular synthesis involving covalent bonds, so inorganic supramolecular compounds may be a new promising IR NLO material system.

To gain further insights on the photonic properties of **1** and **2** and the piezoelectric origin of **2**, theoretical studies including

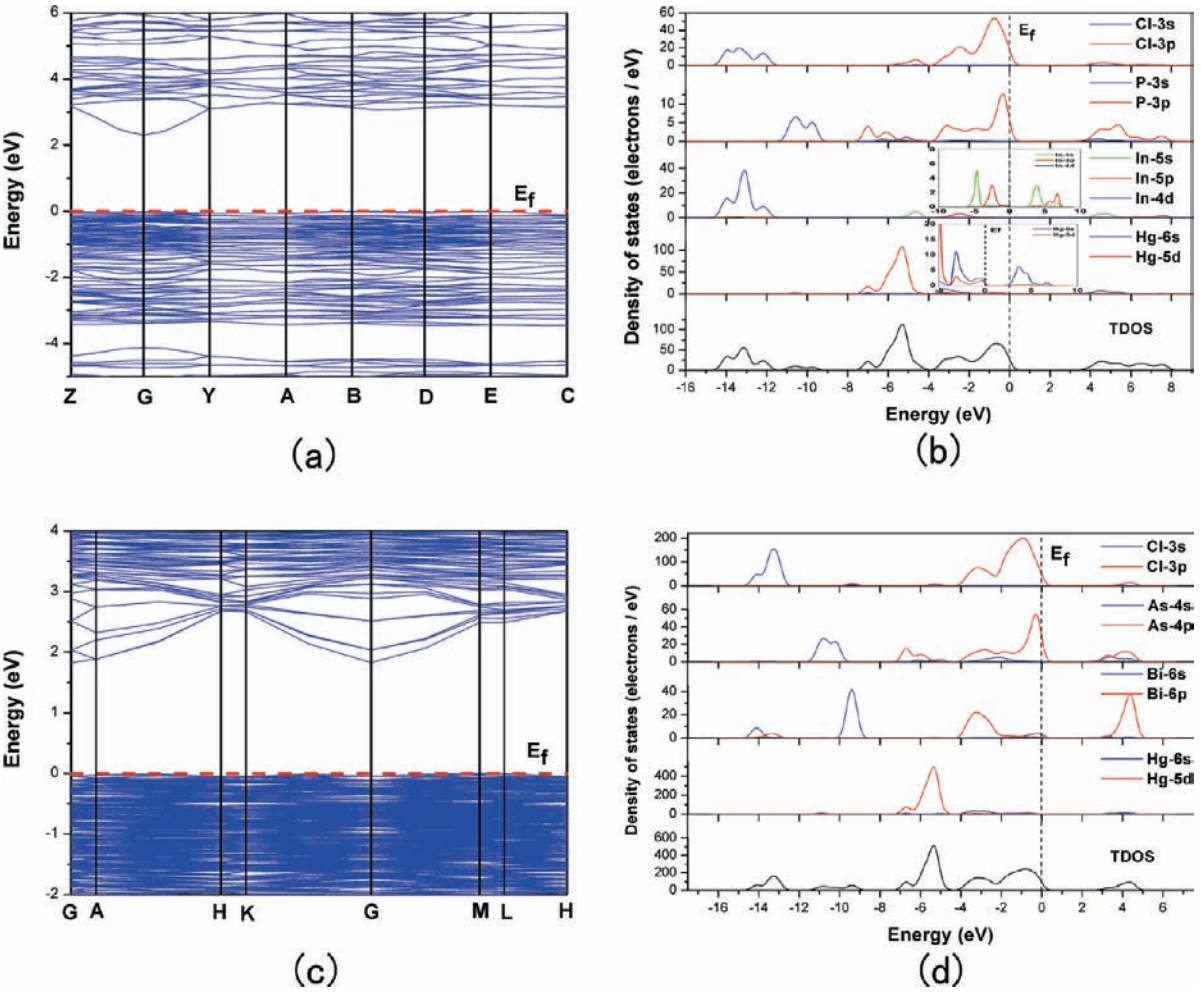

Figure 4. Band structures of **1** (a) and **2** (c) (bands are shown only between −5.0 and 6.0 eV for **1**, and −2.0 and 4.0 eV for **2**, for clarity). Total and partial density of states of **1** (b) and **2** (d); the energies less than −16.0 eV for **1** and −17.5 eV for **2** are omitted for clarity. The Fermi level is set at 0 eV for all the band structures and DOS.

band structure, second-order NLO susceptibility, and piezoelectric constants based on DFPT and $2n+1$ theorem[32,15a,15b] were performed by using the ABINIT computer code package,[17] which is important for understanding the relationship between crystal structure and performances and the design for other complicated IR NLO and piezoelectric materials.

The calculated band structures as well as DOS of **1** and **2** along certain symmetry directions are given in Figure 4. It can be noted from the band structure plots that compounds **1** and **2** are both indirect band gap materials. The band gaps of **1** and **2** using the LDA are E_g = 2.30 and 1.83 eV, which are smaller than the experimental values of 3.13 and 2.43 eV, respectively. So, the scissors operators of 0.83 and 0.60 eV are obtained for calculations of DOS as well as optical properties of **1** and **2**, respectively.

From DOS and PDOS diagrams (Figure 4), it is known that, for **1**, the conductive band (CB) is derived mainly from P-3p and Hg-6s states, mixing with small amounts of Cl-3p, In-5s, and In-5p states, while the valence band (VB) from −8.0 eV to the Fermi level is composed of Cl-3p and Hg-5d states, mixing with small amounts of P-3p, In-5s, and In-5p states. The band from −16.0 to −8.0 eV originates predominately from Cl-3s and In-4d states, as well as a small portion of P-3s states. Therefore, their optical absorptions can mainly be ascribed to the charge transitions from Cl-3p and Hg-5d states to P-3p and Hg-6s states. For **2**, The Cl-3p, As-4p, Bi-6p, and Hg-5d states, mixing with small As-4s states, create the CBs between the Fermi level (0.0 eV) and 6.0 eV. The VBs between −8.0 eV and the Fermi level are mostly formed by Cl-3p and Hg-5d states mixing with a small amount of As-4p and Bi-6p states, and the VBs between −16.0 and −8.0 eV are mostly a contribution from Cl-3s states hybridized with a small amount of As-4s and Bi-6s states. Therefore, the optical absorptions of **2** are mainly ascribed to the charge transitions from Cl-3p and Hg-5d states to Cl-3p, As-4p, Bi-6p, and Hg-5d states.

The calculated imaginary and real parts, $\varepsilon_2(\omega)$ and $\varepsilon_1(\omega)$, respectively, of the frequency-dependent dielectric functions of **1** and **2** are shown in the Supporting Information, Figure S7. It is found from the dispersion of the calculated $\varepsilon_2(\omega)$ spectra that the maximum absorption peaks are located at about 4.75, 5.60, and 6.50 eV for **1** and 3.45, 3.85, and 5.00 eV for **2** in the x, y, and z polarization directions, which are contributed by the charge transfers from Cl-3p and Hg-5d states to P-3p and Hg-6s states and from Cl-3p and As-4p states to Cl-3p, As-4p, Bi-6p, and Hg-5d states, respectively, according to the above DOS analysis.

The space group of **1** belongs to class 2 and has eight nonvanishing second-order susceptibility tensors (χ_{14}, χ_{16}, χ_{21}, χ_{22}, χ_{23}, χ_{25}, χ_{34}, χ_{36}), and the space group of **2** belongs to class

dx.doi.org/10.1021/ja107921a |*J. Am. Chem. Soc.* 2011, 133, 3410–3418

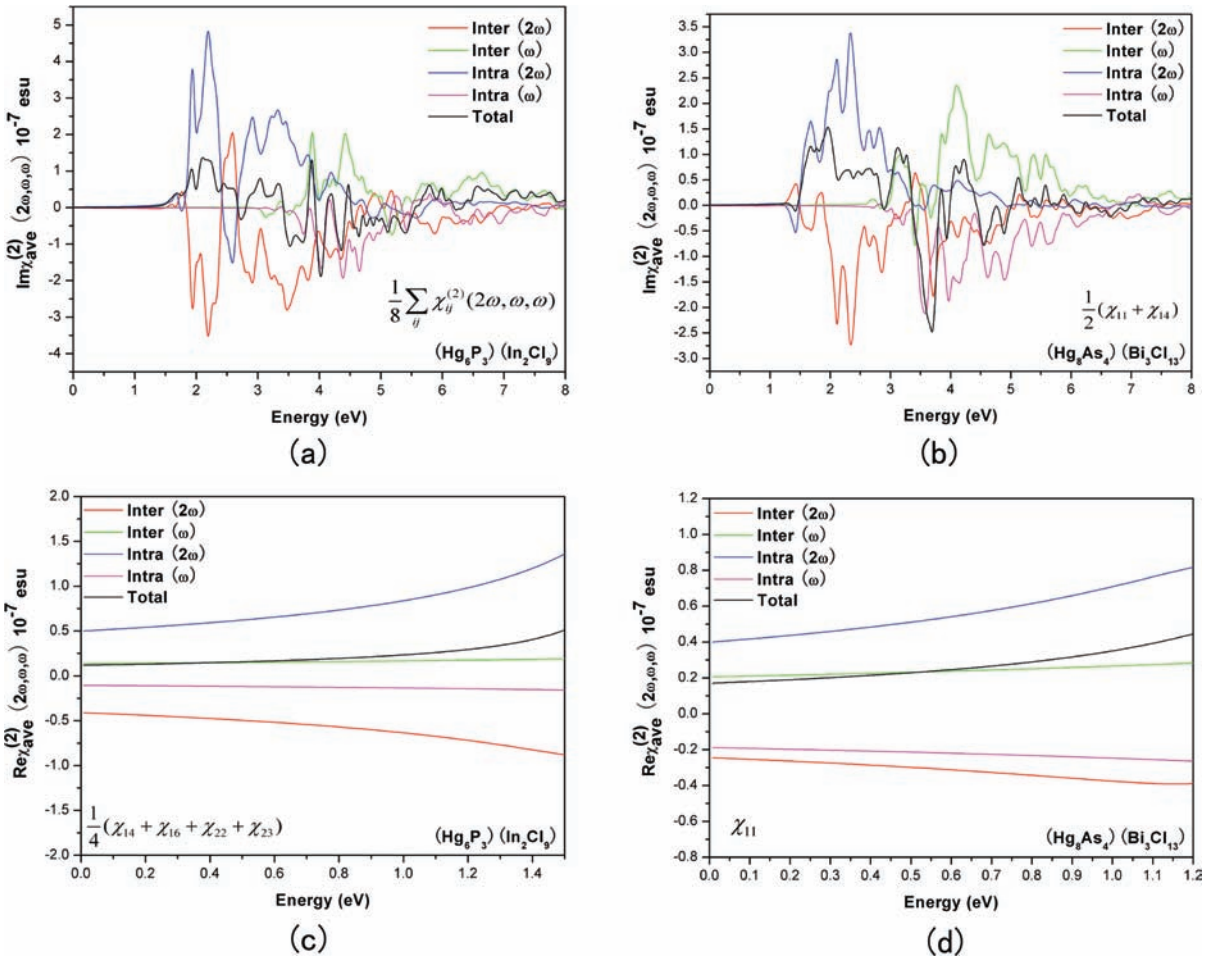

Figure 5. Average imaginary and real parts of second-order susceptibility $\chi^{(2)}_{ave}(2\omega,\omega,\omega)$ of **1** (a, imaginary part; c, real part) and **2** (c, imaginary part; d, real part) and different contributions to them, including the 2ω interband term, the ω interband term, the 2ω intraband term, and the ω intraband term. The energies more than 1.5 eV for **1** and 1.2 eV for **2** are omitted for clarity in the average real part.

32 and has two nonvanishing second-order susceptibility tensors (χ_{11}, χ_{14}). In the low-energy region and under the restriction of Kleinman's symmetry, only four independent SHG tensors (χ_{14}, χ_{16}, χ_{22}, χ_{23}) for **1** and one (χ_{11}) for **2** remain. Different contributions to the real part, $\mathrm{Re}\chi^{(2)}_{ave}(2\omega,\omega,\omega)$, and the imaginary part, $\mathrm{Im}\chi^{(2)}_{ave}(2\omega,\omega,\omega)$, of the average second-order susceptibility $\chi^{(2)}_{ave}(2\omega,\omega,\omega)$, defined as $^1/_8\sum_{ij}\chi^{(2)}_{ij}(2\omega,\omega,\omega)$ for **1** and $^1/_2(\chi_{11}+\chi_{14})$ for **2**, are presented in Figure 5.

The calculated $\mathrm{Im}\chi^{(2)}_{ave}(2\omega,\omega,\omega)$ is zero below half the band gap, as shown in Figure 5. The inter- and intraband 2ω terms start contributing at $\sim^1/_2 E_g$ ($\sim$1.56 eV for **1** and $\sim$1.21 eV for **2**), because the SHG is a two-photon process. Inter- and intraband ω terms contribute for energy values above E_g (3.13 eV for **1** and 2.43 eV for **2**). In the low-energy regime (<3.5 eV for **1** and <3.0 eV for **2**), the SHG optical spectra are dominated by the 2ω contributions. Beyond 3.5 eV for **1** and 3.0 eV for **2**, the major contribution comes from the ω terms.

In the low-energy region (Figure 5c,d), the 2ω interband term and the ω intraband term of $\mathrm{Re}\chi^{(2)}_{ave}(2\omega,\omega,\omega)$ are negative values for both **1** and **2**, while the ω interband term and the 2ω intraband term are positive values. The value of the 2ω intraband term is larger than that of the ω interband term, and the absolute value of the 2ω interband term is larger that that of the ω intraband term in the low-energy region for both **1** and **2**.

The calculated real part of χ_{16}, χ_{14}, χ_{22}, and χ_{23} for **1** at a wavelength of 2.1 μm (0.59 eV) is 0.87×10^{-8}, 2.19×10^{-8}, -2.14×10^{-8}, and 5.75×10^{-8} esu, respectively, and the real part of χ_{11} for **2** is 2.40×10^{-8} esu (Supporting Information, Figure S8). The calculated $\mathrm{Re}\chi^{(2)}_{ave}(2\omega,\omega,\omega)$ values of **1** and **2** are 1.67×10^{-8} and 2.40×10^{-8} esu, respectively, which are on the same order as our experimentally derived χ_{eff} coefficients for **1** (4.24×10^{-8} esu) and **2** (6.57×10^{-8} esu).

Generally, the reported inorganic NLO materials almost always contain a "simple" cation and a SHG-efficient anionic group; single cations with larger ion radius have higher polarizabilities that can make great contributions to the macro-scale SHG efficiency.[33] This work shows, for the first time, that inorganic supramolecular compounds **1** and **2**, containing both complicated polycations and polyanions, exhibit high SHG efficiencies, suggesting that the design of complicated polycations with large molecular polarizability as NLO-phore components should be a useful strategy in searching for new NLO materials.

Compound **2** has two nonvanishing tensors of piezoelectric coefficients, d_{11} and d_{14}, which are calculated to be 1.02 C/m^2 (4.10 pC/N) and 0.33 C/m^2 (30.26 pC/N), respectively, of which the value for d_{11} is close to the experimental value of **2**. Table 2 shows a decomposition of piezoelectric tensors, clearly

dx.doi.org/10.1021/ja107921a |*J. Am. Chem. Soc.* 2011, 133, 3410–3418

Table 2. Decomposition of Piezoelectric Tensors of 2[a]

	$e_{ij,c}$	$e_{ij,int}$	$e_{ij,int,host}$	$e_{ij,int,guest}$	e_{ij}
$i = 1, j = 1$	0.0727	0.9481	0.4558	0.4923	1.0208
$i = 1, j = 4$	0.0319	0.2957	0.0530	0.2427	0.3276

[a] Unit: C/m^2. $e_{ij,c}$, contribution to e_{ij} of vanishing internal strain; $e_{ij,int}$, contribution to e_{ij} of internal strain; $e_{ij,int,host}$, contribution to $e_{ij,int}$ of the host part; and $e_{ij,int,guest}$, contribution to $e_{ij,int}$ of the guest part.

revealing that the main contribution to the piezoelectric effect is the internal strain, to which the host and guest make comparable contributions.

4. CONCLUSIONS

Two novel inorganic supramolecular compounds with 3-D chiral host frameworks have been prepared: **1** and **2** display good IR NLO properties, and **2** shows single-crystal piezoelectric performance. Theoretical studies of the NLO properties for **1** and **2** and piezoelectric properties for **2** show that the larger SHG efficiency of **2** than **1** results from the larger average bond orders of metal−nonmetal bonds in **2** than in **1**, and both the host framework and anionic guest make comparable contributions to the piezoelectric properties of **2**. Our study indicates that good NLO and piezoelectric materials can be obtained by designing both complicated polycations and polyanions with large molecular polarizability as functional components rather than traditional single polyanions, and the spatial arrangement of the functional components can be designed in a reasonable alignment to enforce macroscopic dipole ordering efficiently through crystal engineering strategy.[34]

■ ASSOCIATED CONTENT

Supporting Information. X-ray crystallographic details (CIF); complete ref 17; atomic coordinates, select bond distances lengths, XRD powder patterns, UV diffuse reflectance spectra, TG/DTA mass spectra, coordination geometry of the guests and hosts, calculated imaginary and real parts of dielectric functions, and calculated imaginary and real parts of second-order susceptibilities of $(Hg_6P_3)(In_2Cl_9)$ and $(Hg_8As_4)(Bi_3Cl_{13})$. This material is available free of charge via the Internet at http://pubs.acs.org.

■ AUTHOR INFORMATION

Corresponding Author
gcguo@fjirsm.ac.cn

■ ACKNOWLEDGMENT

We gratefully acknowledge financial support by the NSF of China (20821061, 90922035), 973 program (2011CBA00505), Key Project from the CAS (KJCX2.YW.M10, KJCX2.YW.319), and the NSF of Fujian Province (2008F3115). We thank Fujian Supercomputing Center, Fuzhou University, China, for computer resource support.

■ REFERENCES

(1) (a) Chen, C.; Liu, G. *Annu. Rev. Mater. Sci.* **1986**, *16*, 203. (b) Burland, D. M. *Chem. Rev.* **1994**, *94*, 1. (c) Boyd, G. D.; Buehler, E.; Storz, F. G.; wernick, J. H. *IEEE J. Quantum Electron.* **1972**, *QE 8*, 419. (d) Chen, W.; Mouret, G.; Boucher, D.; Tittel, F. K. *Appl. Phys. B: Laser Opt.* **2001**, *72*, 873.

(2) (a) Halasyamani, P. S.; Poeppelmeier, K. R. *Chem. Mater.* **1998**, *10*, 2753. (b) Zhang, W. G.; Tao, X. T.; Zhang, C. Q.; Gao, Z. L.; Zhang, Y. Z.; Yu, W. T.; Cheng, X. F.; Liu, X. S.; Jiang, M. H. *Cryst. Growth Des.* **2008**, *8*, 304. (c) Liao, J. H.; Marking, G. M.; Hsu, K. F.; Matsushita, Y.; Ewbank, M. D.; Borwick, R.; Cunningham, P.; rosker, M. J.; Kanatzidis, M. G. *J. Am. Chem. Soc.* **2003**, *125*, 9484. (d) Chen, C. T.; Wang, Y. B.; Wu, B. C.; Wu, K. C.; Zeng, W. L.; Yu, L. H. *Nature* **1995**, *373*, 322. (e) Sun, C.-F.; Hu, C.-L.; Xu, X.; Ling, J.-B.; Hu, T.; Kong, F.; Long, X.-F.; Mao, J.-G. *J. Am. Chem. Soc.* **2009**, *131*, 9486. (f) Zhang, G.; Liu, T.; Zhu, T. X.; Qin, J. G.; Wu, Y. C.; Chen, C. T. *Opt. Mater.* **2008**, *31*, 110. (g) Kong, F.; Huang, S.-P.; Sun, Z.-M.; Mao, J.-G.; Cheng, W.-D. *J. Am. Chem. Soc.* **2006**, *128*, 7750. (h) Xu, X.; Wang, S.; Ye, N. *J. Alloys Compd.* **2009**, *481*, 664. (i) Lin, X.; Zhang, G.; Ye, N. *Cryst. Growth Des.* **2009**, *9*, 1186. (j) Becker, P. *Adv. Mater.* **1998**, *10*, 979. (k) Guo, S.-P.; Guo, G.-C.; Wang, M.-S.; Zou, J.-P.; Xu, G.; Wang, G.-J. *Inorg. Chem.* **2009**, *48*, 7059and references therein. (l) Dityatiev, O. A.; Berdonosov, P. S.; Dolgikh, V. A.; Aldous, D. W.; Lightfoot, P. *Solid State Sci.* **2006**, *8*, 830. (m) Goodey, J.; Broussard, J.; Halasyamani, P. S. *Chem. Mater.* **2002**, *14*, 3174.

(3) (a) Eckardt, R. C.; Masuda, H.; Fan, Y. X.; Byer, R. L. *IEEE J. Quantum Electron.* **1990**, *26*, 922. (b) Chen, C. T.; Wu, B. C.; Jiang, A. D.; You, G. M. *Sci. Sin., Ser. B* **1985**, *28*, 235. (c) Chen, C. T.; Wu, Y.; Jiang, A. D.; Wu, B. C.; You, G.; Li, R.; Lin, S. *J. Opt. Soc. Am. B* **1989**, *6*, 616. (d) Wang, S.; Ye, N.; Li, W.; Zhao, D. *J. Am. Chem. Soc.* **2010**, *132*, 8779.

(4) (a) Boyd, G. D.; Buehler, E.; Storz, F. G. *Appl. Phys. Lett.* **1971**, *18*, 301. (b) Boyd, G. D.; Kasper, H.; Mcfee, J. H. *IEEE J. Quantum Electron.* **1971**, *QE 7*, 563. (c) Isaenko, L.; Yelisseyev, A.; Lobanov, S.; Petrov, V.; Rotermund, F.; Zondy, J. J.; Knippels, G. H. M. *Mater. Sci. Semicond. Process.* **2001**, *4*, 665.

(5) (a) Zhang, J.; Su, N. B.; Yang, C. L.; Qin, J. G.; Ye, N.; Wu, B. C.; Chen, C. T. *Proc. SPIE* **1998**, *3556*, 1(Electro-Optic and Second Harmonic Generation Materials, Devices, and Applications II, Beijing, China). (b) Ren, P.; Qin, J. G.; Chen, C. T. *Inorg. Chem.* **2003**, *42*, 8.

(6) (a) Phanon, D.; Bentria, B.; Benbertal, D.; Mosset, A.; Gautier-Luneau, I. *Solid State Sci.* **2006**, *8*, 1466. (b) Phanon, D.; Gautier-Luneau, I. *Angew. Chem., Int. Ed.* **2007**, *46*, 8488.

(7) (a) Kim, Y.; Seo, I. S.; Martin, S. W.; Baek, J.; Halasyamani, P. S.; Arumugam, N.; Steinfink, H. *Chem. Mater.* **2008**, *20*, 6048. (b) Chung, I.; Malliakas, C. D.; Jang, J. I.; Canlas, C. G.; Weliky, D. P.; Kanatzidis, M. G. *J. Am. Chem. Soc.* **2007**, *129*, 14996. (c) Das, S.; Chatterjee, U.; Ghosh, C.; Gangopadhyay, S.; Andreev, Y. M.; Lanskii, G.; Badikov, W. *Opt. Commun.* **2006**, *263*, 352. (d) Bera, T. K.; Jang, J. I.; Ketterson, J. B.; Kanatzidis, M. G. *J. Am. Chem. Soc.* **2009**, *131*, 75. (e) Gitzendanner, R. L.; Spencer, C. M.; Disalvo, F. J.; Pell, M. A.; Ibers, J. A. *J. Solid State Chem.* **1996**, *131*, 399.

(8) Dmitriev, V. G.; Gurzadyan, G. G.; Nikogosyan, D. N. *Handbook of Nonlinear Optical Crystals*, 3rd ed.; Springer: Berlin, 1999.

(9) (a) Muller, A.; Reuter, H.; Dillinger, S. *Angew. Chem., Int. Ed. Engl.* **1995**, *34*, 2328. (b) Desiraju, G. R. *Angew. Chem., Int. Ed. Engl.* **1995**, *34*, 2311.

(10) (a) Lehn, J. M. *Science* **1985**, *227*, 849. (b) Soghomonian, V.; Chen, Q.; Haushalter, R. C.; Zubieta, J.; Oconnor, C. J. *Science* **1993**, *259*, 1596. (c) Natarajan, S.; Mandal, S. *Angew. Chem., Int. Ed.* **2008**, *47*, 4798. (d) Liu, Y.; Wu, L. M.; Li, L. H.; Du, S. W.; Corbett, J. D.; Chen, L. *Angew. Chem., Int. Ed.* **2009**, *48*, 5305. (e) Grosche, F. M.; Yuan, H. Q.; Carrillo-Cabrera, W.; Paschen, S.; Langhammer, C.; Kromer, F.; Sparn, G.; Baenitz, M.; Grin, Yu.; Steglich, F. *Phys. Rev. Lett.* **2001**, *87*, 247003. (f) Pouchard, M.; Cros, C.; Hagenmuller, P.; Reny, E.; Ammar, A.; Menetrier, M.; Bassat, J. M. *Solid State Sci.* **2002**, *4*, 723. (g) Bobev, S.; Sevov, S. C. *J. Am. Chem. Soc.* **1999**, *121*, 3795. (h) Kim, S. J.; Hu, S. Q.; Uher, C.; Hogan, T.; Huang, B. Q.; Corbett, J. D.; Kanatzidis, M. G. *J. Solid State Chem.* **2000**, *153*, 321.

(11) Rigaku. *CrystalClear*, Version 1.3.5; Rigaku Corp.: Tokyo, 2002.

(12) Siemens. *SHELXLTL*, Version 5 Reference Manual; Siemens Energy & Automation Inc.: Madison, WI, 1994.

(13) (a) Wendlandt, W. W.; Hecht, H. G. *Reflectance Spectroscopy*; Interscience Publishers: New York, 1966. (b) Korüm, G. *Reflectance Spectroscopy*; Springer: New York, 1969.
(14) (a) Hohenberg, P.; Kohn, W. *Phys. Rev.* **1964**, *136*, B864. (b) Kohn, W.; Sham, L. J. *Phys. Rev.* **1965**, *140*, A1133.
(15) (a) Gonze, X. *Phys. Rev. A* **1995**, *52*, 1086. (b) Gonze, X. *Phys. Rev. A* **1995**, *52*, 1096. (c) Gonze, X. *Phys. Rev. B* **1997**, *55*, 10337. (d) Gonze, X.; Lee, C. *Phys. Rev. B* **1997**, *55*, 10355. (e) Baroni, S.; de Gironcoli, S.; Dal Corso, A.; Giannozzi, P. *Rev. Mod. Phys.* **2001**, *73*, 515.
(16) (a) Giannozzi, P.; de Gironcoli, S.; Pavone, P.; Baroni, S. *Phys. Rev. B* **1991**, *43*, 7231. (b) Baroni, S.; Giannozzi, P.; Testa, A. *Phys. Rev. Lett.* **1987**, *58*, 1861. (c) de Gironocoli, S.; Baroni, S.; Testa, A. *Phys. Rev. Lett.* **1989**, *62*, 2853.
(17) (a) Gonze, X.; et al. *Comput. Mater. Sci.* **2002**, *25*, 478. (b) Gonze, X.; et al. *Z. Kristallogr.* **2005**, *220*, 558.(c) The ABINIT code is a common project of the Université Catholique de Louvain, Corning Inc., and other contributors (http://www.abinit.org). (d) Goedecker, S. *SIAM J. Sci. Comput.* **1997**, *18*, 1605. (e) Payne, M. C.; Teter, M. P.; Allan, D. C.; Arias, T. A.; Joannopoulos, J. D. *Rev. Mod. Phys.* **1992**, *64*, 1045. (f) Gonze, X. *Phys. Rev. B* **1996**, *54*, 4383. (g) fuchs, M.; Scheffler, M. *Comput. Phys. Commun.* **1999**, *119*, 67. (h) Lee, C.; Gonze, X. *Phys. Rev. B* **1995**, *51*, 8610.
(18) Vanderbilt, D. *Phys. Rev. B* **1990**, *41*, 7892.
(19) (a) Ceperley, D.; Ceperley, D. M. *Phys. Rev. B* **1978**, *18*, 3126. (b) Ceperley, D. M.; Alder, B. J. *Phys. Rev. Lett.* **1980**, *45*, 566. (c) Perdew, J. P.; Wang, Y. *Phys. Rev. B* **1992**, *45*, 13244.
(20) (a) Wu, X.; Vanderbilt, D.; Hamann, D. R. *Phys. Rev. B* **2005**, *72*, 035105. (b) Zhang, T.; Zheng, Y. Q.; Chen, J. J.; Song, L. X.; Shi, E. W. *Jpn. J. Appl. Phys.* **2006**, *45* (Pt. 1), 8755. (c) Dal Corso, A.; Posternak, M.; Resta, R.; Baldereschi, A. *Phys. Rev. B* **1994**, *50*, 10715. (d) Vanderbilt, D. *J. Phys. Chem. Solids* **2000**, *61*, 151.
(21) Blatov, V. A.; Shevchenko, A. P.; Serezhkin, V. N. *J. Appl. Crystallogr.* **2000**, *33*, 1193.
(22) (a) Oleneva, O. S.; Olenev, A. V.; Shestimerova, T. A.; Baranov, A. I.; Dikarev, E. V.; Shevelkov, A. V. *Inorg. Chem.* **2005**, *44*, 9622. (b) Oleneva, O. S.; Shestimerova, T. A.; Dikarev, E. V.; Shevelkov, A. V. *Angew. Chem., Int. Ed.* **2006**, *45*, 7719.
(23) (a) Meyer, G.; Blachnik, R. *Z. Anorg. Allg. Chem.* **1983**, *503*, 126. (b) Beck, H. P.; Wilhelm, D. *Angew. Chem.* **1991**, *103*, 897.
(24) (a) Beck, J.; Neisel, U. *Z. Anorg. Allg. Chem.* **2000**, *626*, 1620. (b) Olenev, A. V.; Oleneva, O. S.; Lindsjo, M.; Kloo, L. A.; Shevelkov, A. V. *Chem.—Eur. J.* **2003**, *9*, 3201. (c) Zou, J.-P.; Wu, D.-S.; Huang, S.-P.; Zhu, J.; Guo, G.-C.; Huang, J.-S. *J. Solid State Chem.* **2007**, *180*, 805. (d) Zou, J.-P.; Li, Y.; Fu, M.-L.; Guo, G.-C.; Xu, G.; Liu, X.-H.; Zhou, W.-W.; Huang, J.-S. *Eur. J. Inorg. Chem.* **2007**, *7*, 977.
(25) (a) Nyburg, S. C.; Ozin, G. A.; Szymanski, J. T. *Acta Crystallogr. B* **1972**, *28*, 2885. (b) Hampel, S.; Schmidt, P.; Ruck, M. *Z. Anorg. Allg. Chem.* **2005**, *631*, 272. (c) Krebs, B.; Hucke, M.; Brendel, C. J. *Angew. Chem., Int. Ed. Engl.* **1982**, *21*, 445. (d) Hampel, S.; Schmidt, P.; Ruck, M. *Z. Anorg. Allg. Chem.* **2005**, *631*, 272. (e) Beck, J.; Brendel, C. J.; Bengtsson-Kloo, L.; Krebs, B.; Mummert, M.; Stankowski, A.; Ulvenlund, S. *Chem. Ber.* **1996**, *129*, 1219.
(26) (a) Shevelkov, A. V.; Dikarev, E. V.; Popovkin, B. A. *J. Solid State Chem.* **1996**, *126*, 324. (b) Olenev, A. V; Shevelkov, A. V; Popovkin, B. A. *J. Solid State Chem.* **1999**, *142*, 14. (c) Shevelkov, A. V.; Dikarev, E. V.; Popovkin, B. A. *Z. Kristallogr.* **1994**, *209*, 583. (d) Shevelkov, A. V.; Dikarev, E. V.; Popovkin, B. A. *J. Solid State Chem.* **1993**, *104*, 177. (e) Ledesert, M.; Rebbah, A.; Labbe, P. H. *Z. Kristallogr.* **1990**, *192*, 223.
(27) Kurtz, S. K.; Perry, T. T. *J. Appl. Phys.* **1968**, *39*, 3798.
(28) Zondy, J.-J.; Touahri, D.; Acef, O. *J. Opt. Soc. Am.* **1997**, *B14*, 2481.
(29) Bechmann, R. *Phys. Rev.* **1958**, *110*, 1060.
(30) Brown, I. D.; Altermatt, D. *Acta Crystallogr.* **1985**, *41*, 244.
(31) (a) Levine, B. F. *Phys. Rev. B* **1973**, *7*, 2600. (b) Chen, C.; Lin, Z.; Wang, Z. *Appl. Phys. B: Laser Opt.* **2005**, *80*, 1.
(32) Gonze, X.; Vigneron, J.-P. *Phys. Rev. B* **1989**, *39*, 13120.
(33) (a) Stucky, G. D.; Phillips, M. L. F.; Gier, T. E. *Chem. Mater.* **1989**, *1*, 492. (b) Banerjee, S.; Malliakas, C. D.; Jang, J. I.; Ketterson, J. B.; Kanatzidis, M. G. *J. Am. Chem. Soc.* **2008**, *130*, 12270.
(34) (a) Rogers, R. D.; Bond, A. H.; Aguinaga, S.; Reyes, A. *J. Am. Chem. Soc.* **1992**, *114*, 2967. (b) Cariati, E.; Ugo, R.; Cariati, F.; Roberto, D.; Masciocchi, N.; Galli, S.; Sironi, A. *Adv. Mater.* **2001**, *13*, 1665. (c) Xu, G.; Li, Y.; Zhou, W.-W.; Wang, G.-J.; Long, X.-F.; Cai, L.-Z.; Wang, M.-S.; Guo, G.-C.; Huang, J.-S.; Bator, G.; Jakubas, R. *J. Mater. Chem.* **2009**, *19*, 2179.